Energy 360 (2026) 141604

Contents lists available at ScienceDirect

Energy

journal homepage: www.elsevier.com/locate/energy

Experimental study on integrated hydrogen-based cooling, heating, and power generation

Alok Kumar *, Savvas A. Tassou, Jose Tavares

Centre for Sustainable Energy Use in Food Chains (CSEF), Department of Mechanical and Aerospace Engineering, Brunel University of London, Uxbridge, Middlesex, UB8 3PH, United Kingdom

ARTICLE INFO

Keywords:
Heating
Cooling
PEM fuel cell
Metal hydride
AEM electrolyser
Refrigerated transport

ABSTRACT

To address rising energy demand and global warming, green hydrogen-based energy systems offer a promising alternative to fossil fuels. This study investigates the coupling of an anion exchange membrane (AEM) electrolyser, metal hydride (MH) storage, and a proton exchange membrane fuel cell (PEMFC) for integrated hydrogen storage, power generation, and thermal management. Hydrogen produced at approximately 35 bar by the electrolyser is stored in a MH reactor, and 1.0 m^3 storage vessel. The hydrogen is then supplied to a 4 kW fuel cell (FC) operating at loads between 1 and 3.5 kW. The MH reactor, based on a shell-and-tube heat exchanger design, contains 20 kg of AB_5 alloy with a hydrogen storage capacity of ~300 g (~1.5 wt.%). Experimental results demonstrate stable system operation, with heating output during the absorption half cycle ranging from ~3.5 to 4.4 MJ for various absorption conditions, and cooling output during desorption varying from ~0.2 to 0.75 kW for load conditions ranging between 1.0 and 3.5 kW. With MH coupling, the FC efficiency reached 53%, with optimal performance observed above 50% load. The results confirm the feasibility of MH-based hydrogen storage systems for combined power, heating, and cooling applications, particularly in transport energy systems.

Nomenclature

Abbreviations			
AEM	Anion Exchange Membrane	PEM	Proton Exchange Membrane
DAQ	Data Acquisition System	PEMFC	PEM Fuel Cell
ECT	Embedded Cooling Tube	SMR	Steam Methane Reforming
FC	Fuel Cell	***Symbols***	
HTF	Heat Transfer Fluid	P_d	Desorption Pressure
LHV	Low Heating Value	P_s	Supply Pressure
MHFC	Metal Hydride Fuel Cell	T_a	Absorption Temperature
MH	Metal Hydride	T_d	Desorption Temperature
PCM	Phase Change Material	wt.%	Weight Percentage of H_2 to MH
PCT	Pressure Concentration Isotherm	η	Efficiency of the Fuel Cell

1. Introduction

The global shift toward low-carbon energy systems has intensified research into efficient methods for hydrogen production, storage, and utilization [1]. Hydrogen is widely recognized as a versatile energy carrier with high gravimetric energy density and zero carbon emissions at the point of use [2]. However, the viability of hydrogen-based energy systems depends strongly on the development of integrated technologies capable of producing, storing, and converting hydrogen in a safe, efficient, and economically feasible manner [3]. As the global demand for sustainable and clean energy sources grows, hydrogen is emerging as a promising energy carrier due to its high energy density and environmentally benign by-products [4,5]. Hydrogen can be produced through several methods, including steam methane reforming (SMR), coal gasification, biomass conversion, water electrolysis, etc [6–8]. Water electrolysis produces hydrogen by splitting water into hydrogen and oxygen using electricity, and when powered by renewable energy sources such as solar, wind, or hydropower, it generates virtually zero greenhouse gas emissions. Although electrolysis is currently more expensive and energy-intensive than conventional methods, its environmental benefits, scalability, high hydrogen purity, and compatibility with renewable energy make it the most sustainable and promising hydrogen production method for a low-carbon future [9]. Among the various electrolysis technologies, hydrogen production using AEM electrolysers is

This article is part of a special issue entitled: ICP2025 - Invitation Only published in Energy.

* Corresponding author.
E-mail address: alok.kumar@brunel.ac.uk (A. Kumar).

https://doi.org/10.1016/j.energy.2026.141604
Received 20 February 2026; Received in revised form 13 May 2026; Accepted 7 June 2026
Available online 8 June 2026

considered a cost-effective approach, as it combines the advantages of both alkaline and PEM electrolysers whilst delivering high-purity hydrogen at lower cost [10,11]. Electrolyser technology plays a crucial role in the production of clean hydrogen, particularly when surplus renewable energy is available. The generated hydrogen can subsequently be utilized to meet energy demands during periods of limited renewable energy supply. Therefore, hydrogen storage serves as an essential link in ensuring a continuous and reliable supply of clean energy [12,13].

Among various hydrogen storage technologies, MH based systems offer a safe, compact, and efficient method for both stationary and mobile applications [14]. These systems utilize reversible chemical reactions between hydrogen and metal alloys to form MH, enabling controlled hydrogen absorption and desorption under moderate temperatures and pressures [15]. These materials absorb hydrogen via reversible chemisorption, enabling stable and long-term storage with minimal losses. Moreover, the exothermic and endothermic thermal phenomena associated with hydrogen absorption and desorption can be harnessed for additional thermal management benefits [16]. A wide range of MH alloys has been extensively investigated for hydrogen storage applications owing to their favourable thermal characteristics [17]. Among these, AB5-type alloys are the most widely studied due to their stability and ability to store hydrogen at relatively low pressure and near-ambient temperature [18]. $LaNi_5$ serves as a base MH material and can be further tailored through elemental substitution to meet specific application requirements. The tailoring characteristics of MH materials makes it flexible to be adopted for various engineering applications such as hydrogen purification, heating, cooling, hydrogen compression, etc. [16]. Liu et al. [19] studied H_2 storage property optimisation of $LaNi_5$ with alloy tailoring through element substitution through modelling and experimental test programme involving substitution of Ni_5 with 8 other elements, Cu, Cr, Mn, Pd, Sn, Zn, Co, and Fe. The results showed, that ball milling and the addition of Cr to $LaNi_5$, led to formation of $LaNi_4Cr$ with improved properties, such as enthalpy of formation compared to the other elements.

Dashbabu and Kumar [20] examined compression performance of tailored AB5 alloy, $LaNi_{5-x}M_x$ (where M = Al, Fe and Mn). Their study was conducted over an absorption temperature range between 20 °C and 40 °C and a desorption range between 80 °C and 140 °C. Within these conditions, $LaNi_{4.8}Al_{0.2}$ achieved the best overall performance and compression ratio of 4.2; however, the storage capacity decreased from 1.4 wt.% to 1 wt.% at the higher absorption temperatures compared to $LaNi_5$. A recent review by Larpruenrudee et al. [21] provides a comprehensive assessment of MH hydrogen storage systems, including their performance and economic aspects. The study also discusses various approaches to enhance reaction kinetics within MH beds, such as the incorporation of fins, metal foams, and phase change materials (PCMs), along with their impact on storage capacity.

MH storage is important due to its potential integration with FC technologies, where the stored hydrogen can be steadily released to generate electricity through electrochemical conversion [22]. This approach is particularly valuable for portable power supplies, backup energy systems, and transportation applications, where reliability and safety are critical. Additionally, the exothermic nature of hydrogen absorption and the endothermic requirement for desorption provide a unique advantage in thermal management and cooling applications [23]. The heat released or absorbed during these processes can be harnessed for thermal energy storage, refrigeration, or waste heat recovery, enhancing the overall efficiency of energy systems [24]. This dual functionality supporting both hydrogen energy supply and thermal regulation positions MH-based storage systems as a versatile and impactful solution in the transition toward a hydrogen-based energy economy.

In 2021, Kolbig et al. [25] reported single and coupled MH reactor systems filled with C5 Hydralloy ($Ti_{0.95}Zr_{0.05}Mn_{1.46}V_{0.45}Fe_{0.09}$) suitable for vehicle cooling applications, along with $LaNi_{4.85}Al_{0.15}$ for lubricant preheating. The investigation targeted a cooling temperature range of 10 °C to −20 °C. On the heating side, the system achieved a specific heating power of 0.5 kW/kg_{MH}, sufficient to raise the temperature of 2 L of lubricant by 20 °C. Similarly, Wimmer et al. [26,27] reported MH based cooling systems for FC electric vehicles. The study reports use of $Ti_{0.99}Zr_{0.01}V_{0.43}Fe_{0.09}Cr_{0.05}Mn_{1.5}$ alloy for high pressure storage, on the MH reactor side and low-pressure usage on the FC side, with pressure ratio of 70 bar to 5 bar (14:1) and facilitating 5 °C cooling temperature. The study reported specific cooling power of 386 W/kg_{MH} at 30 K lift and 229 W/kg_{MH} at 40 K lift respectively. In a subsequent study, Wimmer et al. [27] introduced a novel reactor design incorporating microfluidic channels, achieving an improved specific cooling power of 533 W/kg_{MH}. Melnik et al. [28] reported the coupling of a 1 kW FC with MH-based preheaters to enhance cold-start performance and mitigate FC degradation during operation below 0 °C. The system maintained a stable voltage of 0.6–0.7 V, compared to a drop to 0.45 V without the preheaters. Nyamsi et al. [29], reported theoretical investigation on MH-PCMFC coupling, for light duty vehicle applications. The PCM used in the system facilitated uniform desorption conditions for the MH reactor, causing prolonged desorption at fixed rate. Chabane et al. [30] studied energy management aspects for the coupled MHFC system. The study concludes efficient coupling of MHFC based on required power and thermal behaviour of the FC. Similarly, Parida et al. [22] reports results of experiments on MH system and uses experimental outcomes to simulate PEMFC H2 supply conditions. The study shows, maintaining 40 °C desorption temperature was required to sustain continuous operation of 1 kW FC, with heat input of 125-225 W, highlighting potential thermal coupling.

Integrating hydrogen storage with end-use systems enhances both energy efficiency and system compactness. Coupling a MH storage reactor with a FC allows hydrogen to be released on demand to generate electrical power. The endothermic desorption process can also provide a useful cooling effect, offering a dual function of energy conversion and thermal regulation. When combined with AEM electrolytic hydrogen production, this integrated system represents a closed-loop, flexible, and potentially renewable solution for distributed power generation and thermal management.

Several independent studies have been performed on MH based hydrogen storage systems for various engineering applications [31–36], electrolysers [37–39], and FCs [40–44]. However, only a small number of studies in the literature demonstrate the physical integration of an electrolyser, a MH reactor, and a FC system as a unified setup. This identified research gap, along with the growing need for decarbonized energy systems, highlight the potential practical benefits of such integrated configurations. In particular, the ability to develop a clean energy system capable of delivering multiple outputs presents a promising pathway for future energy solutions. This has served as the primary motivation in defining the objectives of the present work. Considering this research gap, the present study focuses on the experimental investigation of system integration, wherein an AEM electrolyser is coupled with a MH system during the absorption half-cycle, and the MH system is further coupled with a 4 kW PEMFC during the desorption half-cycle. The MH system is filled with 20 kg of $La_xCe_{1-x}(NiCoAl)_5$ with storage capacity of ~3300 l H_2. The experiments were focused on providing efficient coupling at ambient conditions and evaluating the production of cooling and heating to demonstrate the feasibility for mobile refrigeration systems and space heating applications. The research investigates the design, operation, and performance of an integrated energy system comprising an AEM electrolyser for hydrogen production, a MH reactor for storage, and a FC for power generation and auxiliary cooling. The study aims to evaluate system-level behaviour, identify key performance constraints, and provide insights into the techno-thermal interactions that govern overall efficiency. The resulting analysis contributes to the advancement of compact hydrogen-based energy technologies suited for applications in portable power, microgrids, and renewable-energy-powered systems.

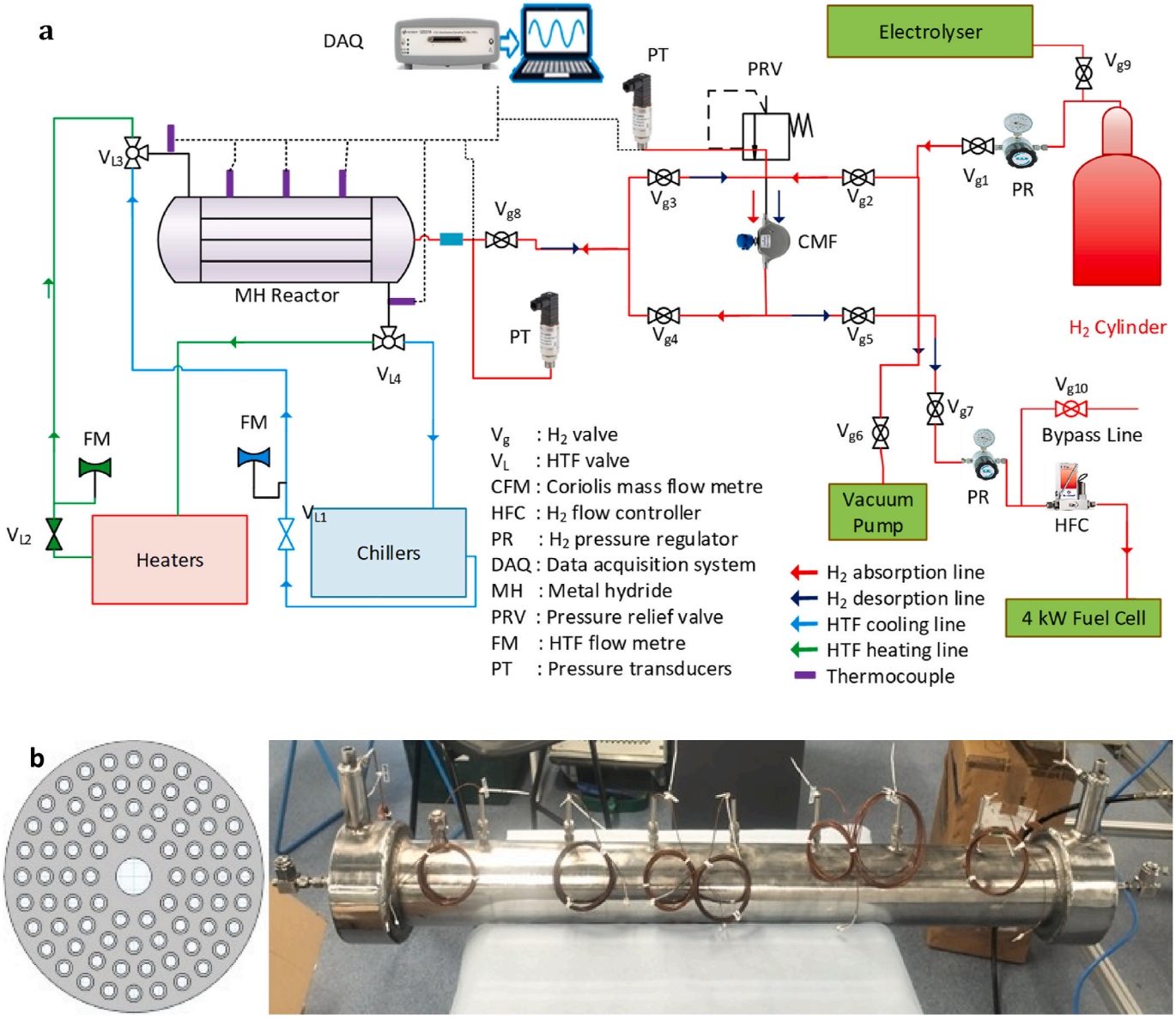

Fig. 1. (a) Schematic diagram of experimental test rig, and (b) Pictorial view of MH reactor.

2. Experimental investigations

As depicted in Figs. 1a and b, the experimental test facility consists of: i) a MH reactor filled with 20 kg $La_xCe_{1-x}(NiCoAl)_5$, ii) a heater and chiller arrangement to facilitate HTF at required temperatures during the experiments, iii) Coriolis mass flow metre to record H_2 flow, iv) HTF flow metre, v) pressure transducers, vi) a data acquisition system, vii) compressed H_2 tank, viii) H_2 pressure regulators, ix) 4 kW PEMFC, x) AEM Electrolyser and, xi) a DC load bank. The gas circuit involves appropriate valving arrangement to direct the flow as per test conditions.

The reactor is of a shell-and-tube arrangement, incorporating 76 embedded cooling tubes (ECTs) to enhance heat removal from the MH bed during hydrogen absorption and desorption processes (Fig. 1b). It was designed to accommodate 20 kg of AB5 alloy, and has dimensions of 1000 mm length and 114.3 mm diameter (schedule 40 pipe). Each ECT had an outer diameter of 6.35 mm and a wall thickness 0.88 mm. A sintered stainless steel (SS316) porous tube with a pore size of 2 μm was installed to facilitate uniform hydrogen supply and discharge within the reactor. This porous element is positioned centrally along the longitudinal axis, serving both as gas distributor and structural support to retain and stabilize the MH alloy within the bed during operation. Hydrogen for the experimental study was generated using an AEM electrolyser operating at a pressure of ~35 bar. The system is comprised of three standard Enapter EL 2.1 stacks connected in parallel, delivering a total hydrogen production capacity of 1500 Nl/h with a purity of 99.99%. The electrolyte used was a 1% KOH solution, with a total deionised water consumption of 1.2 l/h (0.4 l/h per stack), continuously supplied via a deionisation unit. A 4 kW air-cooled PEM electrolyser is employed to power a DC load bank, enabling controlled loading in the range of 1–3.5 kW. This arrangement ensured that the FC operated within a safe and stable regime. The PEMFC system consists of three stacks, each containing 24 cells. For optimal performance, the FC requires a steady hydrogen supply pressure between 0.5 and 0.8 bar, which, during the tests, was maintained using a two-stage pressure regulator on the hydrogen supply line.

Initially, the AEM electrolyser was operated to charge a compressed hydrogen storage tank to a pressure of ~35 bar. This ensured a stable and continuous hydrogen supply to the MH reactor during the experiments. Simultaneously, HTF was circulated through the reactor to

Table 1
Parameters for the experimental study.

Type of study	Operating parameters	System coupled
MH Alloy activation	H_2 supply pressure: ~20 bar Activation Temperature: 5-20 °C HTF flow rate: 5 lpm	MH reactor & AEM Electrolyser
H_2 storage and heating	H_2 supply pressure: 15, 20, & 25 bar Absorption Temperature: 10, 15, & 20 °C HTF flow rate: 10 lpm	MH reactor & AEM Electrolyser
H_2 to power and cooling	H_2 discharge pressure: <0.8 bar (considering FC requirement) Desorption temperature: 25 °C Load: varying between 1 and 3.5 kW Run Time: Up to 1 h HTF flow rate: 10 lpm	MH Reactor & FC

establish the desired absorption temperature conditions. Once a uniform temperature distribution was achieved within the MH bed, hydrogen was introduced into the reactor to initiate the absorption process at a predefined pressure.

The hydrogen supply pressure was regulated using a flow regulator installed in the gas circuit downstream of the storage tank. Hydrogen flow rate was measured using a Coriolis mass flow meter, which provides an accuracy of ±0.25% for H_2 flow at pressures above 1 bar, and measurement precision of 0.01 g $H_2 s^{-1}$. Temperatures within the MH bed, as well as at the HTF inlet and outlet, were monitored using T-type thermocouples, offering an accuracy of ±0.5% and a precision of ±0.5 °C. The internal pressure of the MH reactor was measured using a pressure transducer mounted directly on the reactor, which has an accuracy of ±0.5% with transient response time of 1 ms. The gas circuit incorporated multiple valves to enable flexible flow control depending on the test requirements. A constant-temperature recirculating bath was used to maintain the HTF supply temperature, with a 50% ethylene glycol–water mixture serving as the working fluid. The HTF flow rate was measured using a Picomag flow meter, with an accuracy of ±0.8%, and precision of 0.05 l min^{-1}

All measuring instruments used in the experiments were pre-calibrated for hydrogen gas to ensure reliability and accuracy of the recorded test data. Experimental uncertainty was evaluated using the methodology outlined by Kline and McClintock [45]. The maximum experimental uncertainty in temperature measurement was ±0.5 °C, H_2 flow measurement ±2%, HTF flow ±1.6%, and pressure measurement ±2.5%.

Upon completion of the absorption half-cycle, the reactor temperature was brought to 25 °C using the recirculating temperature bath. For the desorption half-cycle, the reactor outlet was connected to the 4 kW PEMFC, which was connected to a variable DC load bank and a battery system. The hydrogen flow from the reactor to the FC was measured using a Coriolis mass flow meter and regulated using a two-stage pressure regulator. To investigate hydrogen consumption rates under varying operating conditions, the DC load bank was set at different power levels ranging from 1 kW to 3.5 kW across multiple experimental runs. Concurrently, the temperature and pressure within the MH reactor were monitored to evaluate the cooling effect associated with the endothermic desorption process, as well as to quantify the rate of hydrogen consumption. Absorption and desorption half cycles were carried out for a range of parameters depicted in Table 1.

3. Results and discussion

Experiments were performed to activate the MH alloy, and use the MH based hydrogen storage system to run the 4 kW FC under various load conditions. The heating and cooling effects during absorption and desorption half cycles respectively was evaluated to predict the system performance, and feasible coupling with the electrolyzer and FC.

3.1. Alloy selection and activation

Alloy selection for the present study was carried out based on the following considerations:

- High hydrogen storage capacity (~1.5 wt.%): This was a primary consideration to ensure a continuous hydrogen supply to the FC over a relatively extended duration.
- Hydrogen storage at moderate operating conditions: Considering pressure limitation on the H_2 production side (~35 bar), the alloy was selected to have effective hydrogen storage at ~20 bar and ~25 °C absorption conditions.
- Hydrogen discharge at low temperatures: The target discharge pressure was ~5 bar at ~0 °C to enable effective integration with a FC system operating in the range of 0.6–0.8 bar, even under low ambient temperature conditions.
- High enthalpy of hydrogenation/dehydrogenation: To enable efficient recovery of thermal energy in the form of heating and cooling, the alloy was required to maintain sufficiently high reaction enthalpy.
- Low hysteresis: Minimum hysteresis is an important factor to reduce pressure losses during desorption and improve overall system efficiency.
- Ease of activation: The selected MH should be activated easily with available hydrogen pressure at the electrolysers end.

Based on the above selection parameters, MH alloy $La_xCe_{1-x}(NiCoAl)_5$ was tailored and obtained as suitable alloy for the present work.

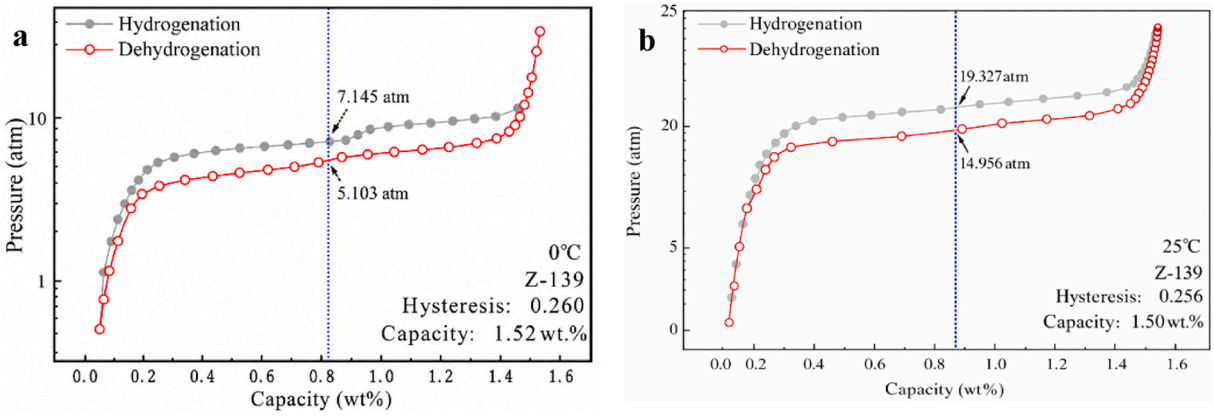

Fig. 2. PCT curve for Z-139 ($La_xCe_{1-x}(NiCoAl)_5$) at (a) 0 °C and (b) 25 °C.

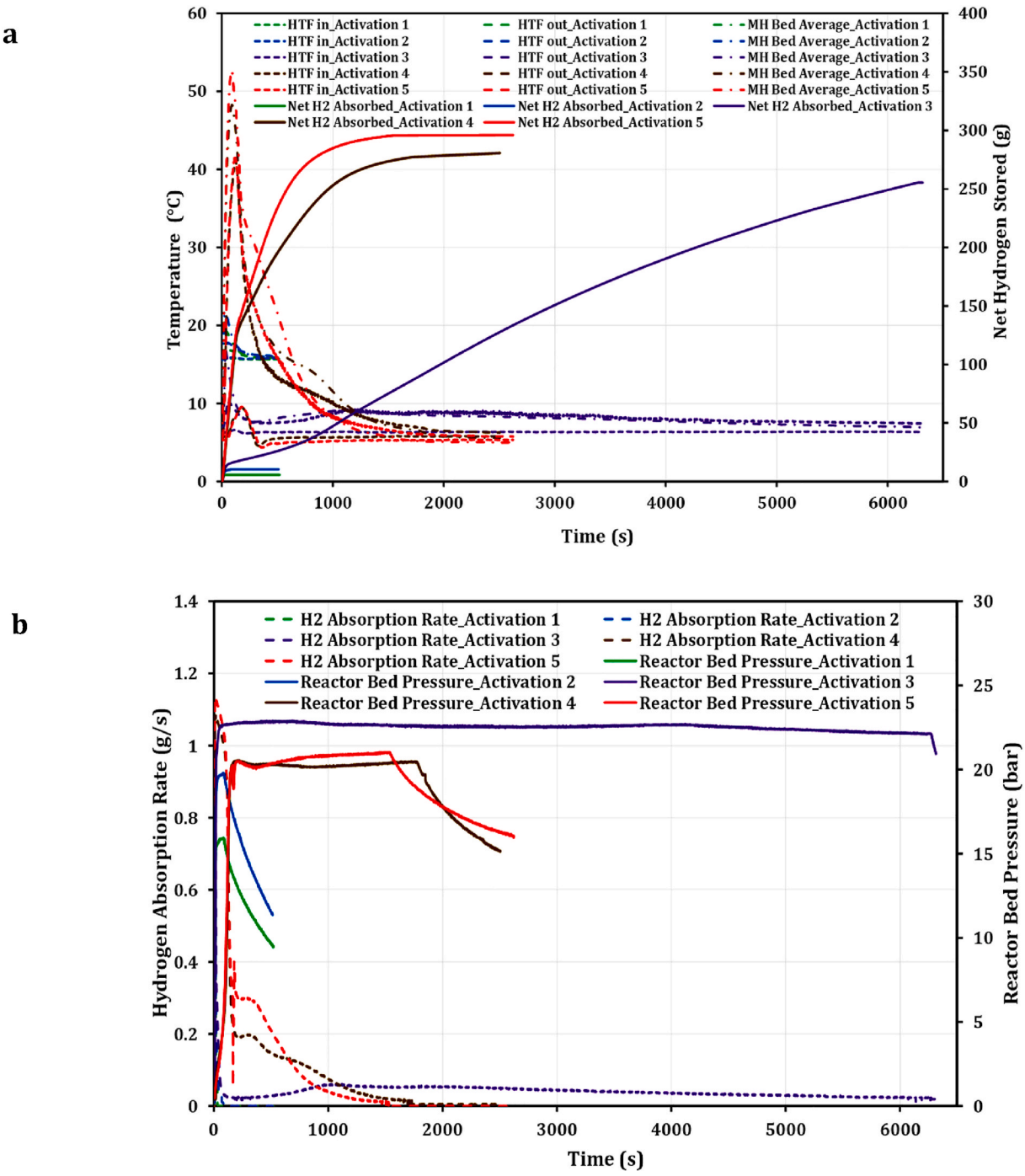

Fig. 3. MH alloy activation curve for (a) temperature variation & net H_2 stored for each activation cycle, and (b) H_2 absorption rate & reactor bed pressure during the activation cycle.

The PCT characteristics of the selected alloy are depicted in Fig. 2.

To activate the MH bed, the reactor was initially heated to 90 °C under vacuum conditions to remove impurities and residual gases. Once a vacuum pressure of 10^{-3} mbar was achieved, the MH bed was cooled down to 15 °C to initiate the first activation cycle. Prior to each activation cycle, the heating and vacuuming procedure was repeated to ensure consistent initial conditions. Once the bed reached a uniform temperature, hydrogen gas at approximately 20 bar was introduced into the reactor. As shown in Figs. 3a and b, the first two activation cycles exhibited minimal hydrogen uptake, with 5.6 g and 10.3 g of hydrogen absorbed, respectively.

Due to the limited hydrogen supply pressure (~35 bar, generated by the AEM electrolyser), the third activation cycle was performed at a reduced bed temperature of 5 °C. Lowering the absorption temperature increased the pressure differential between the MH bed's equilibrium pressure and the hydrogen supply pressure, thereby enhancing the driving force for hydrogen absorption. During the third activation cycle, the MH bed absorbed approximately 255 g of hydrogen in 6300 s, corresponding to ~1.275 wt.% storage capacity. However, the absorption rate was relatively slow, prompting a fourth activation cycle, in which the reactor absorbed 280 g of hydrogen in 2500 s. In the fifth and final activation cycle, the hydrogen absorption further improved, with 295 g absorbed in 1450 s, achieving a storage capacity of ~1.475 wt.%. The peak bed temperature during this cycle reached 52 °C, with a

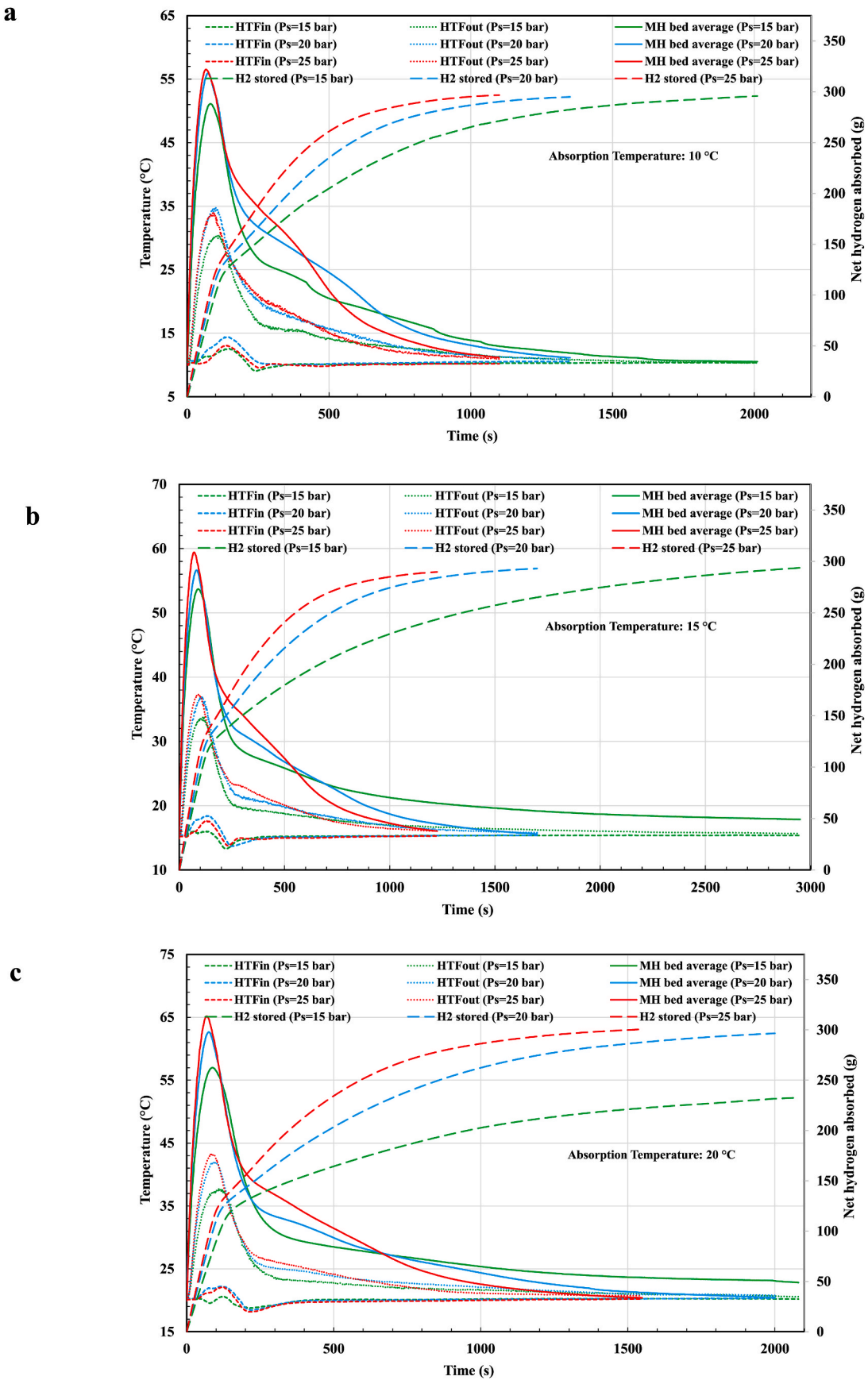

Fig. 4. Effect of H_2 supply pressure on HTF temperature variation and H_2 absorption in the MH reactor for absorption temperatures of (a) 10 °C, (b) 15 °C & (c) 20 °C.

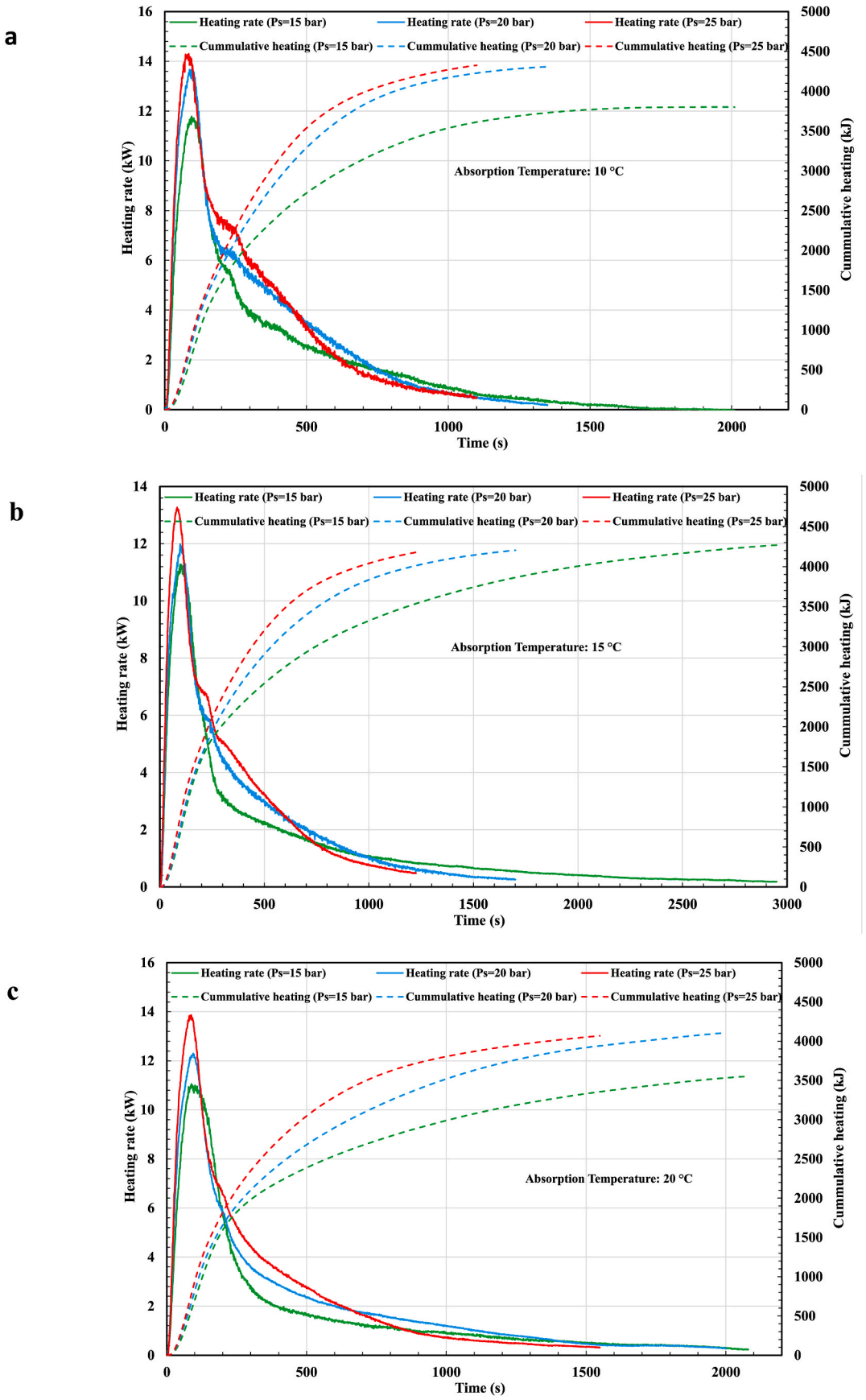

Fig. 5. Effect of absorption pressure on heat output during the absorption process in the MH bed for absorption temperatures of (a) 10 °C, (b) 15 °C & (c) 20 °C.

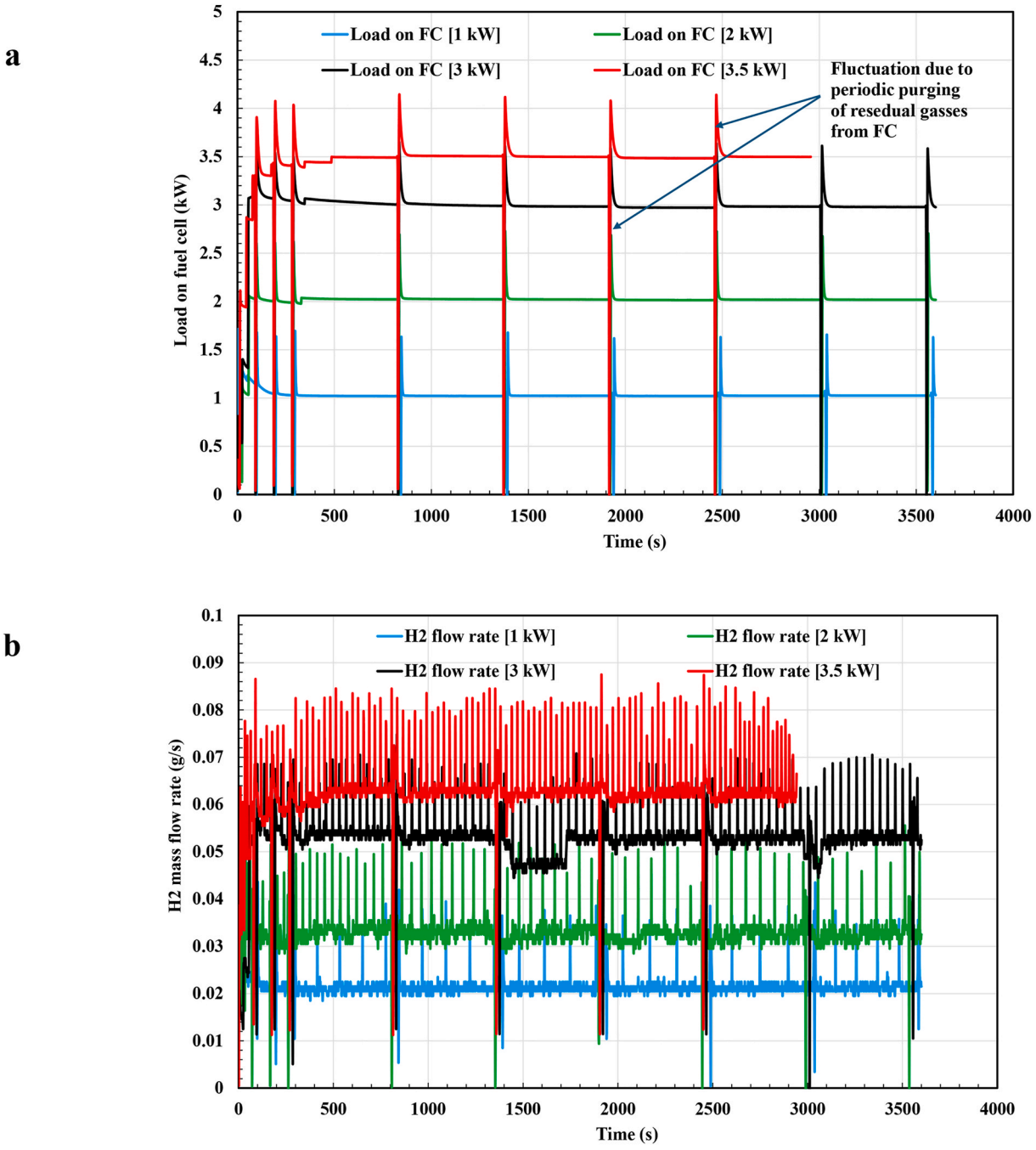

Fig. 6. Plot for (a) DC Load variation during the test run, and (b) corresponding H_2 flow rate for different load conditions.

corresponding HTF outlet temperature of 41 °C. Given that the storage capacity approached the theoretical value, subsequent experiments were conducted with the MH reactor coupled to the PEM FC system.

3.2. Hydrogen Storage and heating

Figs. 4a to c show the effect of variation of the H_2 supply pressure to the MH reactor on H_2 absorption and HTF temperature variation for three absorption temperatures of 10, 15 and 20 °C. Initially, hydrogen was generated by the AEME at ~35 bar. The produced hydrogen was stored in the auxiliary tank and supplied to the MH reactor to maintain the required inlet pressure. For the MH material employed, the equilibrium absorption pressure at 25 °C is approximately 20 bar at the mid-plateau region (Fig. 2b). Consequently, to ensure effective and near-complete hydrogen absorption under the given pressure constraints, operation at lower temperatures becomes necessary. Considering this, the hydrogen absorption experiments were conducted at supply pressures (P_s) of 15, 20, and 25 bar and absorption temperatures (T_a) of 10, 15, and 20 °C to evaluate the absorption kinetics and associated heat generation. All absorption and desorption half-cycle experiments were conducted at a constant HTF flow rate of 10 L min^{-1}. The heating rate was calculated by multiplying the mass flow rate of the HTF by its specific heat and temperature different of the HTF at inlet and outlet of the reactor.

As shown in Fig. 4a, at $T_a = 10$ °C, ~300 g of hydrogen was absorbed for all supply pressures (15, 20, and 25 bar). However, the absorption rate increased with increasing supply pressure. A similar trend was observed at $T_a = 15$ °C (Fig. 4b), where the total hydrogen absorbed

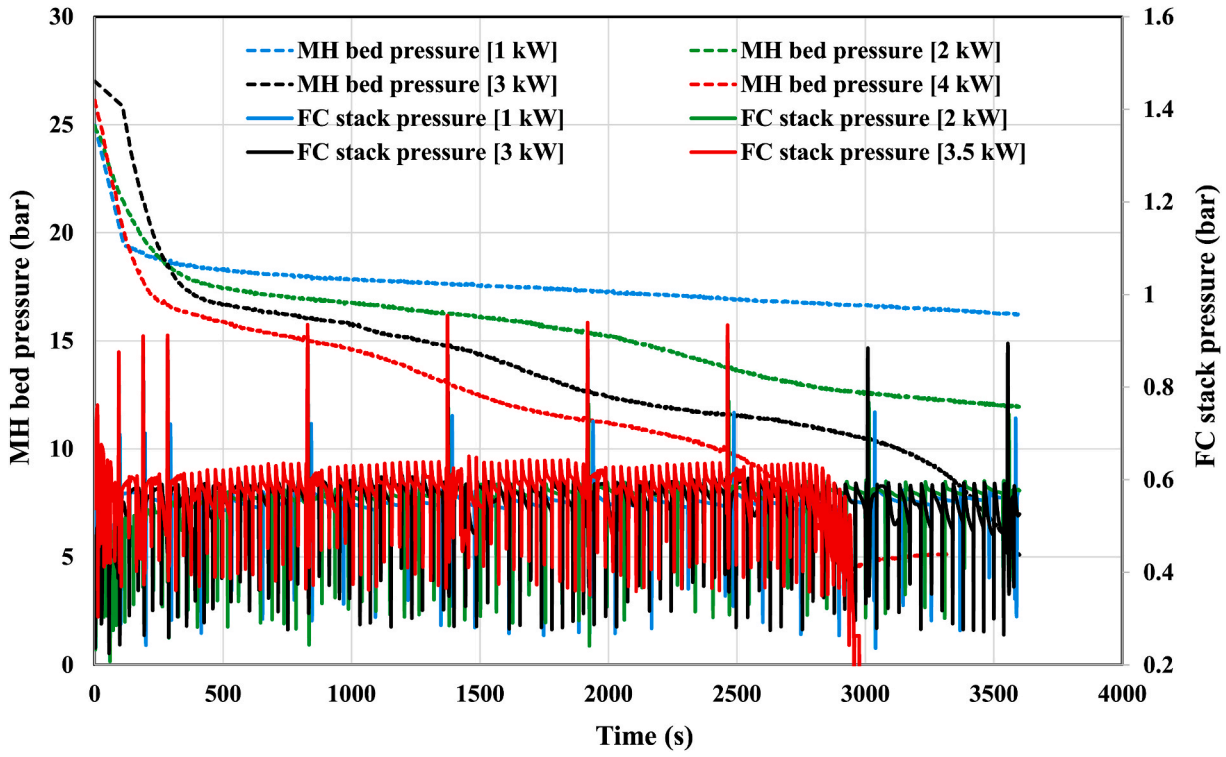

Fig. 7. Variation of MH bed pressure and H_2 pressure at supply of FC under various loads.

remained at ~300 g for all supply pressures. Nevertheless, the absorption rate at $T_a = 10$ °C was consistently higher than that at $T_a = 15$ °C for corresponding supply pressures. The shortest time to reach full absorption was achieved at $P_s = 25$ bar and $T_a = 10$ °C (~1100 s), followed by ~1200 s at $P_s = 25$ bar and $T_a = 15$ °C. This behaviour is attributed to the higher-pressure differential between the hydrogen supply and the equilibrium pressure of the MH bed at lower temperatures i.e 10 °C as compared to 15 °C or 20 °C, resulting in the faster absorption rate. Since the equilibrium pressure of the MH decreases with decreasing temperature, the resulting higher driving force enhances the hydrogen absorption rate.

At $T_a = 20$ °C (Fig. 4c), complete absorption of ~300 g was achieved only for supply pressures of 20 and 25 bar, with the minimum absorption time of ~1550 s at $P_s = 25$ bar. For $P_s = 15$ bar and $T_a = 20$ °C, the pressure difference between the supply and equilibrium bed pressure was insufficient to drive full absorption, resulting in only ~235 g of hydrogen uptake, corresponding to ~78% of the total storage capacity. Therefore, for optimal performance, absorption operation should be performed at supply pressures of 20 to 25 bar and $T_a \leq 20$ °C.

Figs. 5a to c show the variation of the instantaneous and cumulative heat output from the MH reactor during the absorption half cycle for the selected absorption conditions. For most absorption conditions, the cumulative heating output was nearly uniform, ranging between 4200 and 4400 kJ. The consistency in the heating output is due to the similar amount of hydrogen absorbed (~300 g) in each half cycle, and the reaction enthalpy associated with the alloy during the absorption half cycle. However, for $T_a = 20$ °C and $P_s = 15$ bar, the cumulative heating output decreased to ~3500 kJ due to reduced hydrogen absorption under these conditions, which consequently lowered the total heat released, as the net hydrogen absorbed for $T_a = 20$ °C and $P_s = 15$ bar was ~235 g. This left the MH reactor partially unabsorbed to release total heat during the absorption.

The maximum heat output rate was observed at $T_a = 10$ °C and $P_s = 25$ bar, with a peak value of ~14.25 kW and an average heat rate of ~4 kW over an absorption duration of ~1100 s. In contrast, the minimum heat rate for complete hydrogen absorption (~300 g) occurred at $T_a = 10$ °C and $P_s = 15$ bar, yielding a peak heat output rate of ~11.5 kW and an average of ~1.9 kW over a prolonged half-cycle time of ~2020 s. In this case, an estimated heat loss of ~400–500 kJ was observed, primarily due to increased thermal losses at sub-ambient absorption temperatures. This loss corresponds to approximately 10–12% of the net heat generated during ~300 g of hydrogen absorption. However, similar prolonged absorption for $T_a = 15$ °C, and $P_s = 15$ bar was observed (~3000 s), but the heat losses were minimum due to comparatively lesser gap between ambient temperature and experiments.

Overall, the results indicate that hydrogen supply pressure has a significant influence on the average heat output of the system. Higher supply pressure (25 bar in this study) consistently resulted in the highest heat output rates for all three absorption temperatures, with average values ranging from ~2.7 to 4 kW. Therefore, operating the absorption process at higher supply pressures is recommended to ensure a larger thermodynamic driving force for hydrogen uptake, thereby enabling higher and more effective heat output rates.

3.3. Metal hydride-fuel cell coupling study

To investigate the coupling of the MH reactor with a FC power generation system, the MH reactor system was connected to the 4 kW PEMFC. The coupled study was performed at MH desorption temperature of 25 °C to provide sufficient pressure gradient for hydrogen flow from the MH reactor to the PEMFC through the pressure regulators. As depicted in Fig. 6a, for each run, the load on the FC was varied from 1 kW to 3.5 kW. Each test run was performed for ~1 h. Fig. 6b shows, the rate of H_2 mass flow to the FC from the MH reactor, for corresponding load conditions.

During the initial phase of each test run for different load conditions, a slightly higher hydrogen consumption rate was observed. This is attributed to the initial priming of the FC, where residual or diffused atmospheric gases trapped at the anode during the shutdown period were purged and replaced by hydrogen. After this priming phase, hydrogen consumption stabilized in accordance with the applied load. The average hydrogen consumption at 1 kW load was approximately

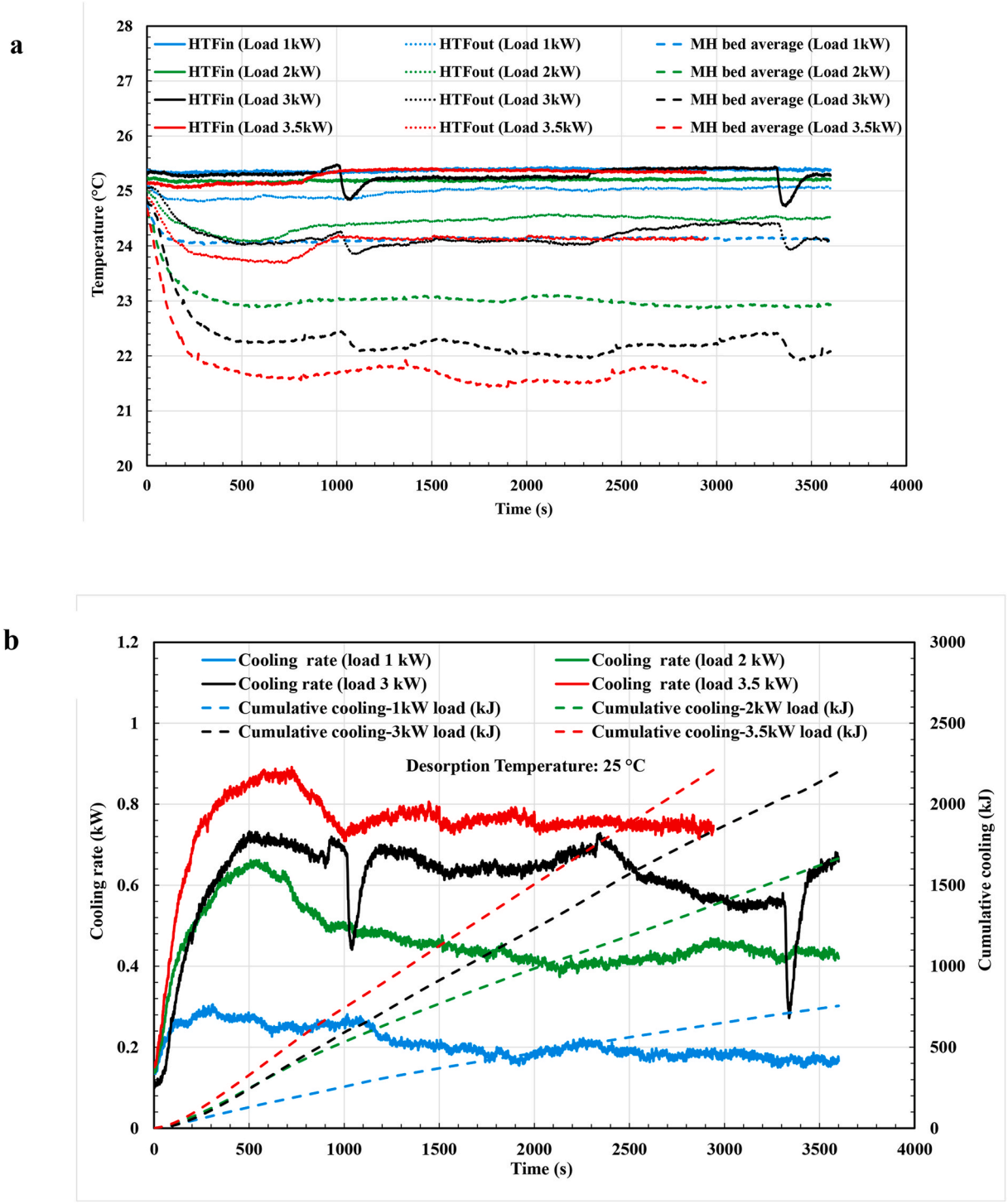

Fig. 8. (a) Variation in the temperature of MH system, and (b) cooling obtained during MH-FC coupling.

0.021 g/s. As expected, the hydrogen consumption rate increased with increasing load: 0.033 g/s at 2 kW, 0.052 g/s at 3 kW, and 0.062 g/s at 3.5 kW. During the FC operation, the system went through automated periodic purging to ensure the isolation of FC from impurities. The effect of these automated flushing of gases causes the data fluctuation, which can be observed in Fig. 6. However, there is no impact on the load, as intermediate fluctuation is taken care of by a secondary battery pack, connected to the FC. At the maximum load of 3.5 kW, the high hydrogen demand led to a significant pressure drop in the MH bed, eventually resulting in inadequate hydrogen supply to the FC and triggering an automatic shutdown to protect the system, after 50 min of operation.

Fig. 7 illustrates the pressure variation within the MH bed, along with the hydrogen supply pressure delivered from the MH reactor to the FC. The required supply pressure for continuous FC operation was maintained within the range of 0.4–0.8 bar. Periodic pressure spikes observed at regular intervals are attributed to the FC purging process, which serves as a protective mechanism to prevent contamination of the FC stack.

It is evident that increasing the electrical load on the FC leads to a corresponding decrease in the MH bed pressure. This behaviour arises from the higher hydrogen flow demand under increased load conditions, which intensifies the endothermic desorption reaction within the MH

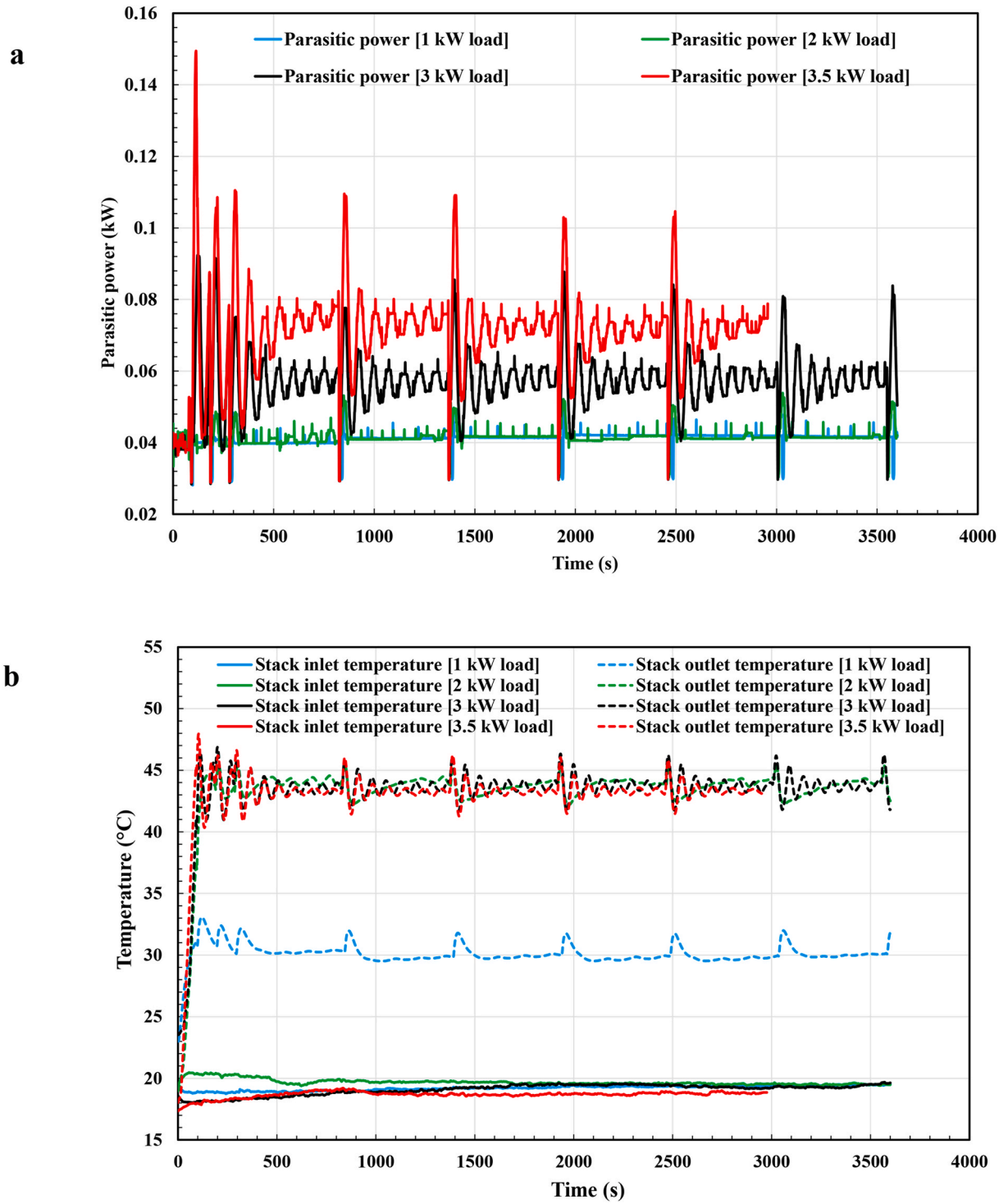

Fig. 9. (a) Plot of parasitic power and (b) FC stack temperature under different load conditions.

bed. The enhanced desorption rate intensifies the endothermic reaction within the MH bed, resulting to a decrease in MH bed temperature, and a simultaneous reduction in the equilibrium bed pressure. Consequently, the available hydrogen pressure at the reactor outlet also decreases. As a result, under higher load conditions of 3.5 kW, the FC operation was terminated before the intended set duration of 1 h due to insufficient hydrogen supply pressure.

Fig. 8a illustrates the variation in MH bed temperature and HTF temperature during FC operation, along with the corresponding cooling effect generated (Fig. 8b), due to endothermic desorption in the MH reactor. The results show that as the load on the FC increased, the temperature drop within both the MH bed and the HTF outlet also increased. This was due to a higher hydrogen desorption rate within the MH reactor to cope with increased hydrogen demand by the FC at elevated loads, which intensified the endothermic reaction and enhanced the cooling effect. The cooling output varied between 0.2 kW and 0.75 kW for load condition of 1 kW to 3.5 kW, with MH bed attaining minimum temperature of ~21.5 °C, and HTF at ~24 °C, for 10 lpm flow. During the initial ~1000 s of operation, the hydrogen desorption rate was higher for all load conditions due to the FC priming

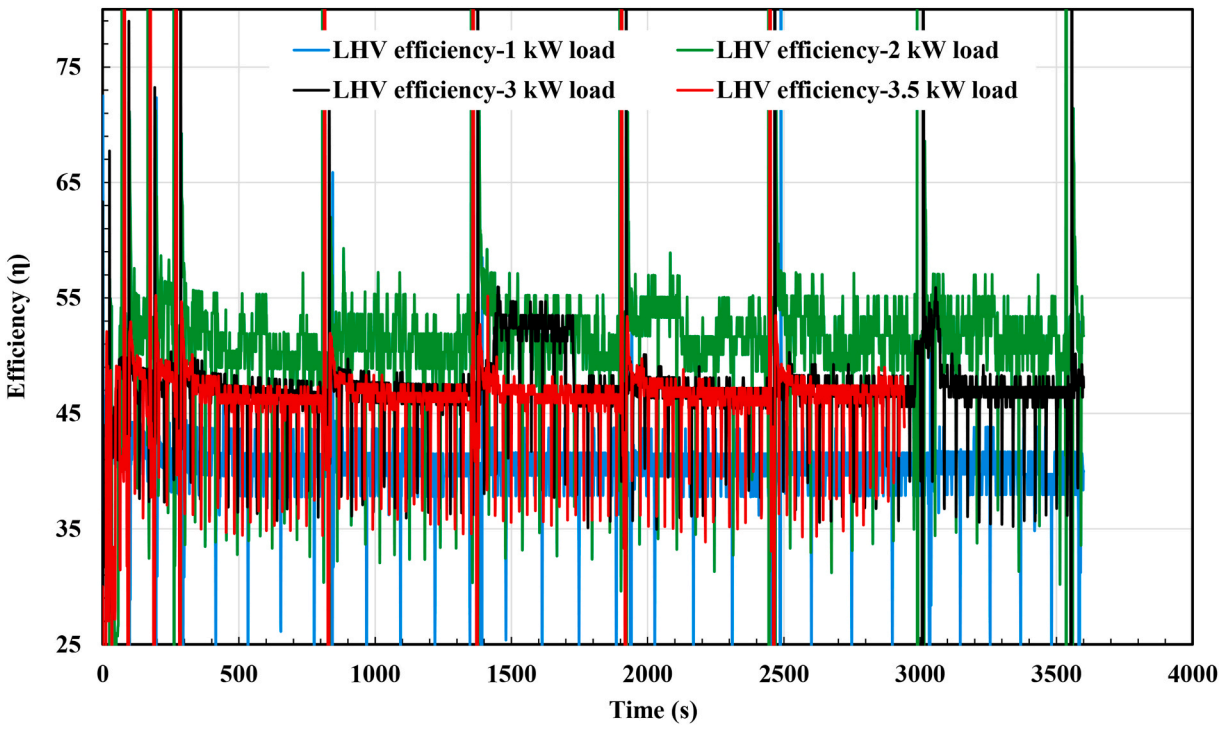

Fig. 10. LHV efficiency of the FC under different load.

phase, during which residual gases from the previous operating cycle were purged. After this transient period, hydrogen consumption stabilized, resulting in a steady desorption rate and a correspondingly stable cooling output for the remainder of the operation. The maximum cumulative cooling was achieved at load conditions of 3 kW and 3.5 kW, with a total cooling output of approximately 2200 kJ.

During FC operation, parasitic losses arise from operation of auxiliary components such as fans, sensors, and control electronics. These additional parasitic loads are illustrated in Figs. 9a and b, show the temperature variation at inlet and outlet of the FC stack with different load.

It can be seen from Fig. 9a, that the parasitic load increased from 0.04 kW to 0.08 kW with increasing load from 1 kW to 3.5 kW, respectively. This trend clearly indicates a direct correlation between the FC load and parasitic power consumption due to increased thermal management requirements. Fig. 9b, shows that increasing the load from 1.0 kW to 3.5 kW increases the stack temperature from approximately 20 °C to 44 °C. For efficient operation of the FC, the maximum stack temperature needs to be maintained between 40 and 45 °C. Higher temperatures necessitate higher rate of cooling, that requires higher fan speed and power consumption.

The FC efficiency under varying load conditions was analysed and is presented in Fig. 10. It was calculated using equation (1), which relates the electrical energy output to the input energy from the hydrogen fuel. The Lower Heating Value (LHV) of hydrogen, 120 MJ/kg was considered in the calculations. Based on the analysis, FC efficiency ranged from 40% to 53%, as the load increased from 1.0 to 3.5 kW.

$$\textit{Fuel cell efficiency} = \frac{\textit{Electrical energy output}}{\textit{Fuel energy } (H_2)} \times 100 \qquad \text{(eq. 1)}$$

It was an interesting observation, that the efficiency near the higher load conditions was higher compared to the lower load case. However, at the peak load of ~90% (3.5 kW), there was a drop in efficiency to 47%. This was due to losses at the gas-catalysis interphase. Additional parasitic losses due to higher fan power to meet FC cooling demand at higher load was also one of the reasons for lower efficiency at ~90% load conditions. It is therefore preferred, for maximum efficiency, to operate the FC between 50 and 75% load conditions.

4. Conclusions

This study demonstrated the effective coupling of a MH storage system with a PEM FC. A total of 20 kg of $La_xCe_{1-x}(NiCoAl)_5$ alloy was filled into a 76 ECT reactor, achieving a hydrogen storage capacity of ~3300 L at 20 bar and 5 °C under activation conditions. The reactor shows maximum cumulative heating output of 4400 kJ, with 4 kW heating rate. The MH system successfully supplied hydrogen to a 4 kW PEM FC under varying load conditions, maintaining continuous operation. Additionally, the system generated a cooling effect of 0.75 kW during operation, demonstrating its potential for simultaneous clean power generation and thermal management.

The FC efficiency ranged between 40% and 53%, based on the LHV of hydrogen and DC load on the FC. For optimal performance and extended system life, it is recommended to operate the FC between 50 and 80% load conditions. Due to the 4 kW load limitation in this study, the hydrogen discharge rate, and consequently the cooling effect was constrained. Coupling the same MH system to a higher-capacity FC could enhance hydrogen discharge and increase the cooling output. Integrating two MH reactors could also enable continuous cooling, making the system suitable for mobile applications, such as refrigeration in refrigerated transport systems.

The material used in the present work limited the cooling delivery temperature to ~5 °C. The use of alternative high pressure and low temperature materials should enable, subzero temperatures to be attained, and larger capacity FCs to be operated. This will be the subject of further investigation to be carried out in the future.

CRediT authorship contribution statement

Alok Kumar: Writing – review & editing, Writing – original draft, Visualization, Validation, Methodology, Investigation, Formal analysis, Data curation, Conceptualization. **Savvas A. Tassou:** Writing – review & editing, Validation, Supervision, Resources, Project administration, Funding acquisition. **Jose Tavares:** Visualization, Investigation, Formal

analysis.

Declaration of competing interest

The authors declare that they have no known competing financial interests or personal relationships that could have appeared to influence the work reported in this paper.

Acknowledgments

The authors would like to acknowledge the funding received from the Engineering and Physical Sciences Research Council (EPSRC), Grant No: EP/T022760/1, H_2-Heat: Thermal energy transport for heating and cooling with innovative hydrogen (H2) technologies, for this project.

Data availability

Data will be made available on request.

References

[1] Ren L, Zhang K, Mehran K, Ma K. Low-carbon economic dispatch of a hydrogen-based integrated energy system considering the coordinated operation of CHP-ORC-CSP and P2G-CCS. Energy 2025;340:139251. https://doi.org/10.1016/J.ENERGY.2025.139251.
[2] Oshiro K, Fujimori S. Role of hydrogen-based energy carriers as an alternative option to reduce residual emissions associated with mid-century decarbonization goals. Appl Energy 2022;313:118803. https://doi.org/10.1016/j.apenergy.2022.118803.
[3] Egeland-Eriksen T, Hajizadeh A, Sartori S. Hydrogen-based systems for integration of renewable energy in power systems: achievements and perspectives. Int J Hydrogen Energy 2021;46:31963–83. https://doi.org/10.1016/j.ijhydene.2021.06.218.
[4] Winter CJ. Hydrogen energy — abundant, efficient, clean: a debate over the energy-system-of-change. Int J Hydrogen Energy 2009;34:S1–52. https://doi.org/10.1016/J.IJHYDENE.2009.05.063.
[5] Li X, Raorane CJ, Xia C, Wu Y, Tran TKN, Khademi T. Latest approaches on green hydrogen as a potential source of renewable energy towards sustainable energy: spotlighting of recent innovations, challenges, and future insights. Fuel 2023;334:126684. https://doi.org/10.1016/J.FUEL.2022.126684.
[6] Singla MK, Gupta J, Beryozkina S, Safaraliev M, Singh M. The colorful economics of hydrogen: assessing the costs and viability of different hydrogen production methods - a review. Int J Hydrogen Energy 2024;61:664–77. https://doi.org/10.1016/J.IJHYDENE.2024.02.255.
[7] Aydin MI, Dincer I. An assessment study on various clean hydrogen production methods. Energy 2022;245:123090. https://doi.org/10.1016/J.ENERGY.2021.123090.
[8] Szablowski L, Wojcik M, Dybinski O. Review of steam methane reforming as a method of hydrogen production. Energy 2025;316:134540. https://doi.org/10.1016/J.ENERGY.2025.134540.
[9] Ji M, Wang J. Review and comparison of various hydrogen production methods based on costs and life cycle impact assessment indicators. Int J Hydrogen Energy 2021;46:38612–35. https://doi.org/10.1016/j.ijhydene.2021.09.142.
[10] Vincent I, Bessarabov D. Low cost hydrogen production by anion exchange membrane electrolysis: a review. Renew Sustain Energy Rev 2018;81:1690–704. https://doi.org/10.1016/j.rser.2017.05.258.
[11] Loh A, Li X, Sluijter S, Shirvanian P, Lai Q, Liang Y. Design and Scale-Up of zero-gap AEM water electrolysers for hydrogen production. Hydrogen (Switzerland) 2023;4:257–71. https://doi.org/10.3390/hydrogen4020018.
[12] Abdalla AM, Hossain S, Nisfindy OB, Azad AT, Dawood M, Azad AK. Hydrogen production, storage, transportation and key challenges with applications: a review. Energy Convers Manag 2018;165:602–27. https://doi.org/10.1016/j.enconman.2018.03.088.
[13] Rasul MG, Hazrat MA, Sattar MA, Jahirul MI, Shearer MJ. The future of hydrogen: challenges on production, storage and applications. Energy Convers Manag 2022;272. https://doi.org/10.1016/j.enconman.2022.116326.
[14] Kumar A, Muthukumar P, Sharma P, Kumar EA. Absorption based solid state hydrogen storage system: a review. Sustain Energy Technol Assessments 2022;52:102204. https://doi.org/10.1016/j.seta.2022.102204.
[15] Baniasadi E, Taheri Z, Kumar A. Energy management in hydrogen energy systems. Reference module in Earth systems and environmental sciences. 2025. https://doi.org/10.1016/B978-0-44-313219-3.00154-4.
[16] Muthukumar P, Kumar A, Raju NN, Malleswararao K, Rahman MM. A critical review on design aspects and developmental status of metal hydride based thermal machines. Int J Hydrogen Energy 2018;43:17753–79. https://doi.org/10.1016/j.ijhydene.2018.07.157.
[17] Muthukumar P, Abraham K, Prasad UAR, Maiya MP, Murthy SS. Screening of metal hydrides for engineering applications. In: Proceedings of ECOS 2003, the 16th international conference on efficiency, cost, optimization, simulation, and environmental impact of energy systems: Copenhagen, Denmark, June 30 - july 2, 2003; 2003.
[18] Mani N, Ramaprabhu S. Effect of substitutional elements on hydrogen absorption properties in Mm-based AB5 alloys. J Alloys Compd 2004;363:275–91. https://doi.org/10.1016/S0925-8388(03)00487-0.
[19] Liu Y, Chabane D, Elkedim O. Optimization of LaNi5 hydrogen storage properties by the combination of mechanical alloying and element substitution. Int J Hydrogen Energy 2024;53:394–402. https://doi.org/10.1016/J.IJHYDENE.2023.12.038.
[20] Dashbabu D, Anil Kumar E. Analytical and experimental evaluation of LaNi5-xMx, where M = Fe, Mn, and Al hydrides for hydrogen compression applications. Therm Sci Eng Prog 2024;51:102624. https://doi.org/10.1016/J.TSEP.2024.102624.
[21] Larpruenrudee P, Bennett NS, Luo Z, Hossain MJ, Haque N, Sauret E, et al. A review on the overall performance of metal hydride-based hydrogen storage systems. Energies 2025;18:1291. https://doi.org/10.3390/EN18051291. 2025;18:1291.
[22] Parida A, Kumar A, Muthukumar P, Dalal A. Experimental and numerical investigations on synergistic coupling of metal hydride hydrogen storage systems with low-temperature proton exchange membrane fuel-cell. Therm Sci Eng Prog 2024;51:102620. https://doi.org/10.1016/j.tsep.2024.102620.
[23] Kumar A, Raju NN, Muthukumar P. Parametric studies on MmNi4.7Fe0.3 based reactor with embedded cooling tubes for hydrogen storage and cooling application. J Energy Storage 2021;35:102317. https://doi.org/10.1016/j.est.2021.102317.
[24] Jenne SP, Jana S, Palanisamy M. Thermal and compressor-driven metal hydride based coupled system for thermal storage, cooling and thermal upgradation. Therm Sci Eng Prog 2021;21. https://doi.org/10.1016/j.tsep.2020.100800.
[25] Kölbig M, Bürger I, Linder M. Thermal applications in vehicles using hydralloy C5 in single and coupled metal hydride systems. Appl Energy 2021;287. https://doi.org/10.1016/j.apenergy.2021.116534.
[26] Wimmer A, Linder M, Bürger I. Metal hydride-based cooling system for fuel cell electric vehicles: achieving a temperature lift of 40 K. Appl Energy 2025;398:126396. https://doi.org/10.1016/J.APENERGY.2025.126396.
[27] Wimmer A, Kordel M, Linder M, Bürger I. High performance reactor of a metal hydride based cooling system for air-conditioning of fuel cell electric vehicles. Appl Energy 2025;391:125911. https://doi.org/10.1016/J.APENERGY.2025.125911.
[28] Melnik D, Bürger I, Mitzel J, Käß J, Sarkezi-Selsky P, Jahnke T, et al. Energy efficient cold start of a polymer electrolyte membrane fuel cell coupled to a thermochemical metal hydride preheater. Appl Energy 2024;359:122585. https://doi.org/10.1016/j.apenergy.2023.122585.
[29] Nyamsi SN, Tolj I, Gęca MJ. Dehydrogenation of metal hydride reactor-phase change materials coupled with light-duty fuel cell vehicles. Energies 2022;15. https://doi.org/10.3390/en15092982.
[30] Chabane D, Ibrahim M, Harel F, Djerdir A, Candusso D, Elkedim O. Energy management of a thermally coupled fuel cell system and metal hydride tank. Int J Hydrogen Energy 2019;44:27553–63. https://doi.org/10.1016/j.ijhydene.2019.08.247.
[31] Kumar A, Muthukumar P. Experimental studies on poisoning of La0.9Ce0.1Ni5 based hydrogen purification system with CO2 as impurity. Int J Hydrogen Energy 2023;48:37774–83. https://doi.org/10.1016/j.ijhydene.2022.10.137.
[32] Muthukumar P, Groll M. Metal hydride based heating and cooling systems: a review. Int J Hydrogen Energy 2010;35:3817–31. https://doi.org/10.1016/J.IJHYDENE.2010.01.115.
[33] Anbarasu S, Muthukumar P, Mishra SC. Tests on LmNi4.91Sn0.15 based solid state hydrogen storage device with embedded cooling tubes - part B: desorption process. Int J Hydrogen Energy 2014;39:4966–72. https://doi.org/10.1016/j.ijhydene.2014.01.039.
[34] Satheesh A, Muthukumar P. Performance investigation of double-stage metal hydride based heat pump. Appl Therm Eng 2010;30:2698–707. https://doi.org/10.1016/j.applthermaleng.2010.07.021.
[35] Sreeraj R, Aadhithiyan AK, Anbarasu S. Integration of thermal augmentation methods in hydride beds for metal hydride based hydrogen storage systems: review and recommendation. J Energy Storage 2022;52:105039. https://doi.org/10.1016/j.est.2022.105039.
[36] Sharma VK, Kumar EA. Thermodynamic analysis of novel multi stage multi effect metal hydride based thermodynamic system for simultaneous cooling, heat pumping and heat transformation. Int J Hydrogen Energy 2017;42:437–47. https://doi.org/10.1016/J.IJHYDENE.2016.09.154.
[37] Guo X, Zhu H, Zhang S. Overview of electrolyser and hydrogen production power supply from industrial perspective. Int J Hydrogen Energy 2024;49:1048–59. https://doi.org/10.1016/j.ijhydene.2023.10.325.
[38] Ferriday TB, Sampathkumar SN, Middleton PH, Kolhe ML, Van Herle J. A review of membrane electrode assemblies for the anion exchange membrane water electrolyser: perspective on activity and stability. Int J Energy Res 2024;2024. https://doi.org/10.1155/2024/7856850.
[39] Ratib MK, Muttaqi KM, Islam MR, Sutanto D, Agalgaonkar AP. Large-scale production of green hydrogen from solar energy in Australia: operation and control of a multi-unit PEM electrolyser system. Int J Hydrogen Energy 2025;98:873–86. https://doi.org/10.1016/j.ijhydene.2024.10.281.
[40] Ministry of Economy Trade and Industry. Strategy for developing hydrogen and fuel-cell technologies formulated, 1–2. Trade and Industry: Ministry of Economy; 2019.
[41] Yatoo MA, Habib F, Malik AH, Qazi MJ, Ahmad S, Ganayee MA, et al. Solid-oxide fuel cells: a critical review of materials for cell components. MRS Commun 2023;13:378–84. https://doi.org/10.1557/s43579-023-00371-0.

[42] Stambouli AB. Fuel cells: the expectations for an environmental-friendly and sustainable source of energy. Renew Sustain Energy Rev 2011;15:4507–20. https://doi.org/10.1016/j.rser.2011.07.100.
[43] Athanasaki G, Jayakumar A, Kannan AM. Gas diffusion layers for PEM fuel cells: materials, properties and manufacturing – a review. Int J Hydrogen Energy 2023; 48:2294–313. https://doi.org/10.1016/j.ijhydene.2022.10.058.
[44] Barbir F. Chapter 11 - fuel cells and hydrogen economy. In: Barbir F, editor. PEM fuel cells. Burlington: Academic Press; 2005. p. 399–426. https://doi.org/10.1016/B978-012078142-3/50012-4.
[45] Kline SJ, McClintock FA. Describing uncertainties in single-sample experiments. Mech Eng 1953;75:3–8.